



Contents lists available at ScienceDirect

Physics Letters A

www.elsevier.com/locate/pla

The characteristics of surface arc plasma and its control effect on supersonic flow

Quan Sun^a, Yinghong Li^a, Bangqin Cheng^a, Wei Cui^{b,*}, Wendi Liu^c, Qing Xiao^c^a Science and Technology on Plasma Dynamics Laboratory, School of Aeronautics and Astronautics Engineering, Air Force Engineering University, Xi'an, China^b School of Aerospace Engineering, Tsinghua University, Beijing, China^c Department of Naval Architecture, Ocean and Marine Engineering, University of Strathclyde, Glasgow, United Kingdom

ARTICLE INFO

Article history:

Received 9 April 2014

Received in revised form 11 June 2014

Accepted 13 July 2014

Available online xxxxx

Communicated by F. Porcelli

Keywords:

Surface arc plasma

Discharge characteristic

Supersonic

Shock wave

Flow control

ABSTRACT

The characteristic of surface arc plasma included millisecond and microsecond actuation in supersonic flow is investigated both experimentally and numerically. In the experiment, the discharge characteristic of surface arc plasma in quiescent air and supersonic flow is recorded. The stable oblique shock could be observed with millisecond actuation. And the unstable compressive wave could be also observed with microsecond actuation. In the numerical investigation, plasma actuation is defined as a source term with input power density from discharge $V-I$ characteristic, which is expected to better describe the influence of heating process. The numerical results are coincident with experimental results. In order to confirm the capability of surface arc plasma actuation to control supersonic flow, experimental investigations on control shock induced by ramp and separation of boundary layer induced by impinging shock are performed. All the results demonstrate the control effect of surface arc plasma actuation onto supersonic flow.

© 2014 Elsevier B.V. All rights reserved.

1. Introduction

Shockwave is the typical aerodynamic phenomenon in supersonic flow, and if controlled effectively, a series of potential applications can be achieved, such as reducing the wave drag. The wave drag has great influence on the flight performance of the aircrafts and can consume a large proportion of the fuel. Therefore, to reduce fuel consumption and to increase the aircraft range as well as supersonic cruise, the reduction of wave drag has become an important issue. Shockwave-boundary layer interactions (SWB-LIs) commonly occur in high-speed flows from the transonic to the hypersonic regime. They can be found in a variety of applications including transonic wings, axial turbines, and mixed-compression inlets. The interaction often results in performance detriments because the boundary layer must negotiate the imposed adverse pressure gradient. The effect of the adverse pressure gradient of the boundary layer can cause separation. These effects (especially the increased unsteadiness and aerodynamic blockage associated with separation) have the potential to reduce system performance significantly.

Shockwave and boundary layer control can be achieved by many mechanical and aerodynamic methods, such as the ramp

angle control in supersonic inlet and the vortex generators control in self-adapted wing. Because the mechanical configuration is complex and the flow control response is slow, plasma flow control method has become the research hotspot in the international aerodynamics and thermodynamic field and is expected to bring significant benefits for aircraft such as improved performance and lower cost [1–5]. It has many advantages such as simple structure, flexible control and excitation frequency bandwidth.

The experimental investigation on shock control by plasma aerodynamic actuation was carried out at High Temperature Research Institute in Russian Academy of Sciences [6,7]. The results of experiments showed that, after using the plasma aerodynamic actuation, it could induce weakly oblique shock and reduce the angle and intensity of shock wave in supersonic flow. State University of New Jersey in the United States carried out experimental and numerical studies of shock control by the plasma aerodynamic actuation [8,9]. They applied cylinder model to generate detached shock and employed pulsed microwave discharge to produce plasma. The results of experiments showed that, with plasma aerodynamic actuation, the normal shock intensity at the center place of detached shock was weakened and shock shape was bended. Meyer et al. [10] investigated whether the control process of shock was dominated by the thermal or ionization mechanism through plasma aerodynamic actuation.

* Corresponding author.

E-mail address: cw14@mails.tsinghua.edu.cn (W. Cui).

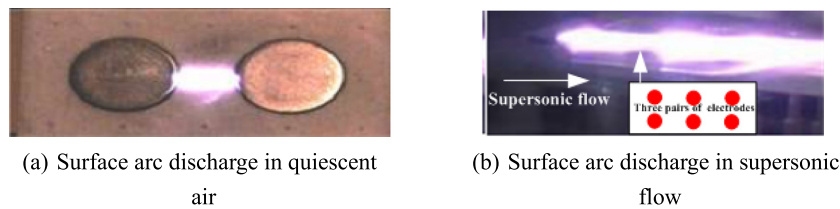


Fig. 1. The discharge picture with surface arc plasma.

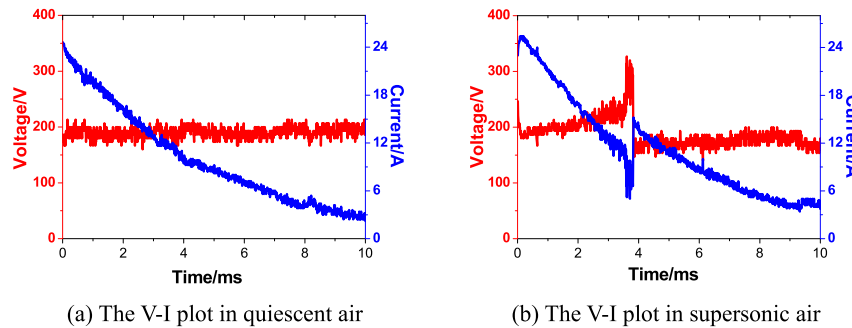


Fig. 2. The $V-I$ plot with discharge voltage of 1 kV.

Recently, localized arc filament plasma actuators (LAPPAs) were developed at the Ohio State University as a means to introduce strong, tailored, high frequency perturbations to flow [11–14]. They forced incoming boundary layer at a frequency close to one of the instability frequencies associated with the reflected shock interacting with the unsteady separation bubble. This resulted in reduction of the separation bubble size and reflected shock unsteadiness. For the mechanism of flow control, they could not reach an agreement between Joule heating effect and unsteadiness manipulation effect. Separation bubble forcing was also performed using a magnetically driven gliding arc to modify static pressure distributions downstream and modulate the flow in the separation region [15, 16]. Using an upstream-directed Lorentz force at low discharge currents (80 mA), it was able to create a local separation bubble for incipient SWBLIs. At higher discharge current (200 mA) and with downstream-directed Lorentz forcing, they were able to demonstrate a considerable reduction in the length scale of the separation bubble. Another approach used a pulsed plasma jet to force an oblique shock on a compression ramp in a Mach 3 flow [17]. It was reported that convection of thermal spots in the incoming boundary layer displaces the oblique shock location upstream, while forcing in the separation bubble did not produce a detectable effect. In addition, the researchers found that, when actuation was used at the upstream of the shock, it was possible to lock the low-frequency instability movement of the shock, effectively reduced the flowing pressure fluctuations near the wall. Flow forcing by repetitive thermal perturbations in NS-DBD actuators was applied for SWBLIs [18]. The main idea of this approach was forcing the flow with high amplitude, high bandwidth perturbations, at a frequency approaching one of flow instability frequencies, thus triggering their subsequent growth in the flow. These results suggest that plasma-induced shockwave-boundary layer flow forcing may have a potential for high-speed flow control applications.

Surface arc plasma actuators have also been developed at the Science and Technology on Plasma Dynamics Laboratory at the Air Force Engineering University in China [19–22]. In the present work, the characteristic of surface arc plasma included millisecond and microsecond actuation in supersonic flow is investigated both experimentally and numerically. Through the modeling of electrical heating, the arc domain is defined a source term with input power density from discharge $V-I$ characteristic, which is expected to better describe the influence of heating process. At

last, experimental investigations on control shock induced by ramp and separation of boundary layer induced by impinging shock are performed. All the results demonstrate the control authority of surface arc plasma actuation onto supersonic flow.

2. The discharge characteristics affected by supersonic flow

The shape of arc plasma is shown in Fig. 1 from top view. From Fig. 1(a), we can see that the discharge arc is strongly bounded near the wall surface. The inner layer of discharge arc is white which indicates the plasma temperature is very high, but the outer layer is blue and purple because of its weak discharge intensity. There are three pairs of electrodes in supersonic flow. Compared with quiescent flow, we can observe that arc discharge spreads the whole electrodes areas from Fig. 1(b), which is strongly blown downstream by the supersonic gas flow, and it's a large-area surface discharge near the wall.

2.1. The discharge characteristics of millisecond actuation

The design Mach number of the small-scale short-duration supersonic wind tunnel is 3 and its steady operation time is about 60 milliseconds. The test section is rectangular with 100 mm wide and 30 mm high. The gas static pressure and static temperature in the test section are 2813 Pa and 105 K respectively. The groove in the test section lower wall is designed for the plasma actuator fabrication. Plasma actuator consists of a pair of electrodes and the insulating dielectric. The electrodes are made of copper, and flush-mounted on the top wall of the insulating dielectric. The diameter of the electrode is 10 mm. The insulating dielectric is made of BN (Boron Nitride) ceramic.

The plasma power source adopts pulsed DC power source which consists high voltage pulsed circuit, high voltage DC circuit and feedback circuit. The high voltage pulsed circuit breakdowns the gas and this step lasts extremely short time of about 1 microsecond. The second step is the DC hold-up process and maintains about 10 milliseconds.

The electrical parameter measurement system includes DPO4104 oscilloscope, P6015A high voltage probe and TCPA300 + TCP312 current probe for measuring voltage and current.

Fig. 2(a) is the discharge characteristics in quiescent air. This curve contains only the high-voltage DC discharge. When applying

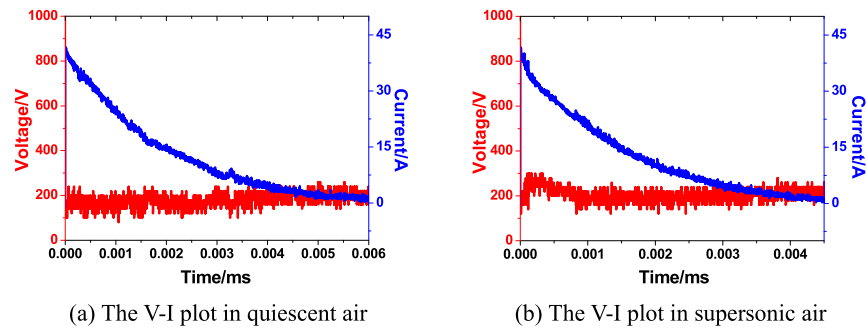


Fig. 3. The $V-I$ plot with discharge frequency of 1 kHz and voltage of 15 kV.

actuation voltage of 1000 V, DC discharge voltage drops instantly from 1000 V to 200 V and lasts about 10 milliseconds. And the current is dropped from 24 A at the beginning to 3 A. The average power is about 2.7 kW and the energy is approximately 27 J. Fig. 2(b) is the discharge characteristics in supersonic flow ($M = 3$). Compared with discharge characteristics in quiescent air, when applying actuation voltage of 1000 V, DC discharge voltage drops instantly from 1000 V to 200 V and lasts about 4 milliseconds. And the current is dropped from 24 A at the beginning to 3 A. An interesting phenomenon occurs. The supersonic flow blows out the discharge. Then the discharge continues and lasts 6 milliseconds. With the energy consumption of capacitance, the discharge current and intensity get decreased until the discharge disappears. In this process, the average power is about 2 kW and the energy is approximately 20 J.

2.2. The discharge characteristics of microsecond actuation

In order to investigate different actuation times of surface arc discharge, the plasma power source also adopts microsecond actuation. The principle of discharge is similarity with millisecond actuation. The plasma power source is high-voltage pulse ionization and DC discharge maintained. The DC hold-up process is about 10 microseconds. And the discharge actuation frequency varies from 100 Hz to 2000 Hz.

Fig. 3(a) is the discharge characteristics in quiescent air. This curve contains only single the high-voltage DC discharge. When applying actuation voltage of 15 kV and frequency of 1 kHz, DC discharge voltage drops instantly to 200 V and lasts about 6 microseconds. And the current is dropped from 36 A at the beginning to 0. The average power is about 3.6 kW and the energy is approximately 2.1 mJ. Fig. 3(b) is the discharge characteristics in supersonic flow ($M = 3$). Compared with discharge characteristics in quiescent air, when applying actuation voltage of 15 kV, DC discharge voltage drops instantly to 200 V and lasts about 5 milliseconds. And the current is dropped from 36 A at the beginning to 0. And this process, the supersonic flow cannot blow out the discharge. The average power is about 3.6 kW and the energy is approximately 1.8 mJ.

It can be concluded from the comparison above that, in supersonic flow, the DC discharge of millisecond actuation is unstable, and the discharge channel cannot be maintained. The main reason for this phenomenon is that the heating is not dissipated immediately as soon as the arc plasma extinguish. Then this heating effect breakdowns the medium to generate arc relying on the action of thermal energy. In the quiescent condition, there is a path between the two electrodes after the last discharge where the temperature is higher and the intensity of activity particles is higher, it should be a preferential way for the next arc. But in the supersonic flow, heat and particles were blown by the flow. So the same energy cost could sustain longer discharge time in the quiescent condition than the supersonic ones. Such an explanation corresponds

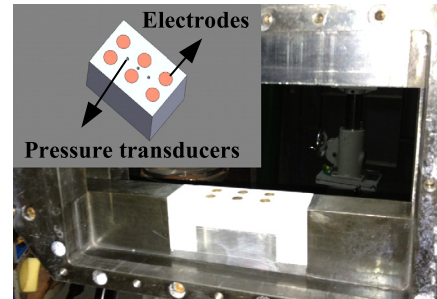


Fig. 4. Test section of shock induced by surface arc discharge.

to the microseconds of time between the extinguishment and the reappearance of the arc. But in supersonic flow, the DC discharge of microsecond actuation is stable. The discharge power input has changed with higher discharge current, that is, the microsecond actuation can stable the arc.

3. The flow field characteristics affected by surface arc discharge

Due to the short time of wind tunnel experiment, the parameter measurement system should have a higher response frequency. The piezoelectric sensor is the ICP (integrated circuit piezoelectric) sensor of PCB. The response frequency of pressure transducers is 100 kHz. The schlieren system uses the high-speed CCD camera with the maximum frame frequency of 200 000 fps. For the purpose of acquiring the pulsed discharge process, the frame frequency in this paper is selected as 20 000 fps (frame interval of 50 μ s), and the resolution is 512 \times 218 pixels.

Accurate synchronous control is needed in the experiment. Synchronous control system, including impedance matching and channel decelerator, is the control hub of the entire experimental system. The output signal of the sensor is passed to the synchronization control system through the constant current source, and is magnified to the channel decelerator through impedance matching. Set the accurate delay of every experimental system and parametric test system, and carry out the accurate control and parameter diagnose for plasma flow control experiments.

3.1. The oblique shock induced by millisecond actuation

Experimental investigation on inducing shock by millisecond plasma actuation is performed in small-scale short-duration supersonic wind tunnel. The designed Mach number of supersonic wind tunnel is 3 and its steady operation time is about 60 ms. The gas static pressure and static temperature in the test section are 2813 Pa and 105 K respectively.

It uses the second pair electrodes to discharge and first and third pressure transducers to measure wall static pressure in Fig. 4. Fig. 5(a) and Fig. 5(b) are the flow benchmark picture and with

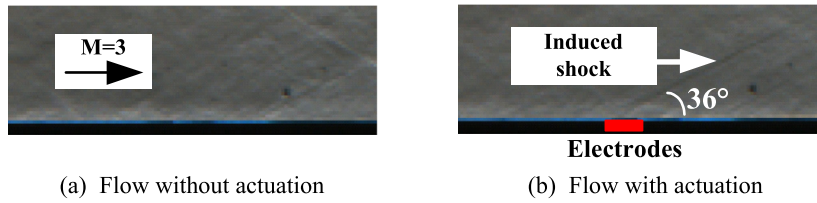


Fig. 5. Schlieren images of shock induced in Mach 3 flow.

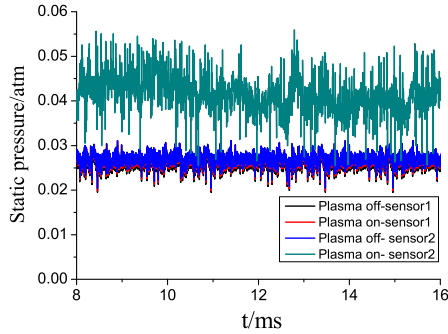


Fig. 6. Static pressure compared with millisecond actuation.

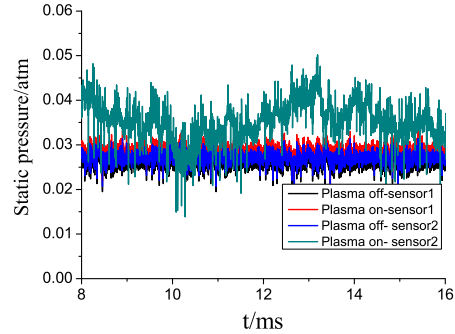


Fig. 8. Static pressure compared with microsecond actuation.

millisecond plasma actuation picture which delays 3 millisecond after plasma discharge. When the actuation is applied and actuation voltage of 1000 V, the shock wave is generated due to Joule heating in the discharge area.

Fig. 6 is wall static pressure measured by pressure sensors (sensor 1, sensor 2) before and behind discharge area. From the figure, it can be found that the static pressure values of sensor 1 and sensor 2 are approximately same without plasma actuation. The static pressure of sensor 2 increases when applying plasma actuation. The reason is that the flow velocity decreases due to Joule heating and inducing shock wave.

3.2. The compressive wave induced by microsecond actuation

In order to investigate different actuation times to disturb the supersonic flow by surface arc discharge, the plasma power source adopts microsecond actuation. The gas static pressure and static temperature in the test section are 2813 Pa and 105 K respectively.

Fig. 7(a) and Fig. 7(b) are the flow field pictures with microsecond plasma actuation which delay 50 μs and 1100 μs after plasma discharge. When the plasma actuation is applied and actuation voltage of 15 kV and frequency of 1 kHz, compression wave generated by the pulse discharge in the actuator is readily apparent in supersonic flow.

Fig. 8 is wall static pressure measured by pressure sensors (sensor 1, sensor 2) before and behind discharge area. Compared with millisecond plasma actuation, the static pressure of sensor 2 (after discharge area) increases less and becomes unstable. The pressure distributing is not dithering with pulse repeated voltage of microsecond actuation. The reason maybe that the frequency of PCB transducers is not so high that follow the respond time of flow field.

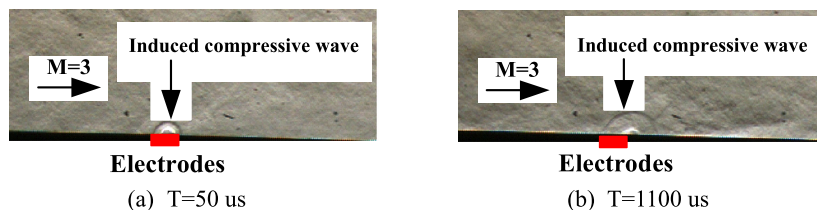


Fig. 7. Schlieren images of compressive shock induced in Mach 3 flow.

4. Numerical model and simulation

In order to better understand the mechanism and character of surface arc discharge in supersonic flow, numerical investigations have also been finished. After the modeling of arc plasma, the commercial computational fluid dynamics flow solver is adopted for calculation.

4.1. Numerical model

The present simulation is based on solving Reynolds averaged Naviere Stokes equations (URANS). The governing equations for compressible flow associated with mass, moment and energy conservation are as follows:

$$\frac{\partial}{\partial t} \int_V \mathbf{W} dV + \oint [F - G] \cdot dA = \int_V H dV \tag{1}$$

where V is an arbitrary control volume with differential surface area dA . The vectors \mathbf{W} , \mathbf{F} , \mathbf{G} and source term \mathbf{H} are defined as:

$$\mathbf{W} = \begin{Bmatrix} \rho \\ \rho u \\ \rho v \\ \rho w \\ \rho E \end{Bmatrix}, \quad \mathbf{F} = \begin{Bmatrix} \rho v u + p \hat{i} \\ \rho v v + p \hat{j} \\ \rho v w + p \hat{k} \\ \rho v E + p v \end{Bmatrix}, \tag{2}$$

$$\mathbf{G} = \begin{Bmatrix} 0 \\ \tau_{xi} \\ \tau_{yi} \\ \tau_{zi} \\ \tau_{ij} v_j + q \end{Bmatrix}, \quad \mathbf{H} = \begin{Bmatrix} 0 \\ M_x \\ M_y \\ M_z \\ E_s \end{Bmatrix}$$

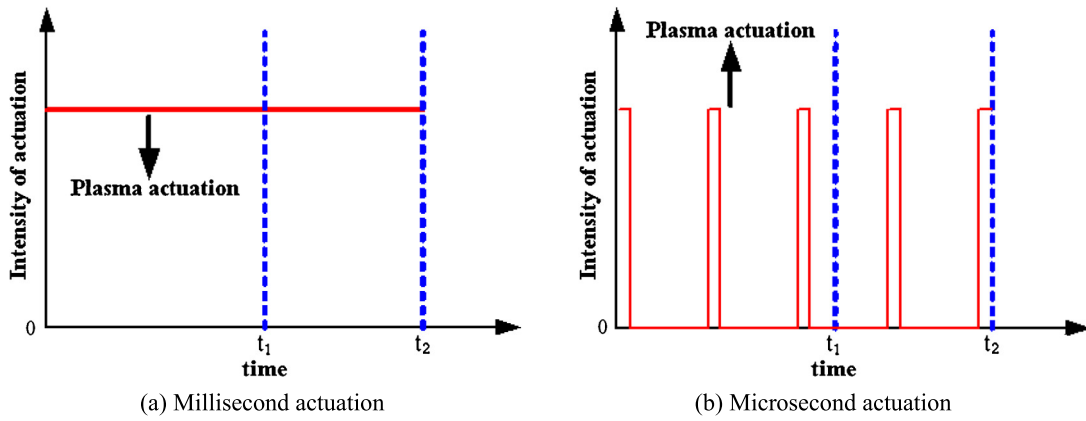


Fig. 9. Intensity actuation plots.

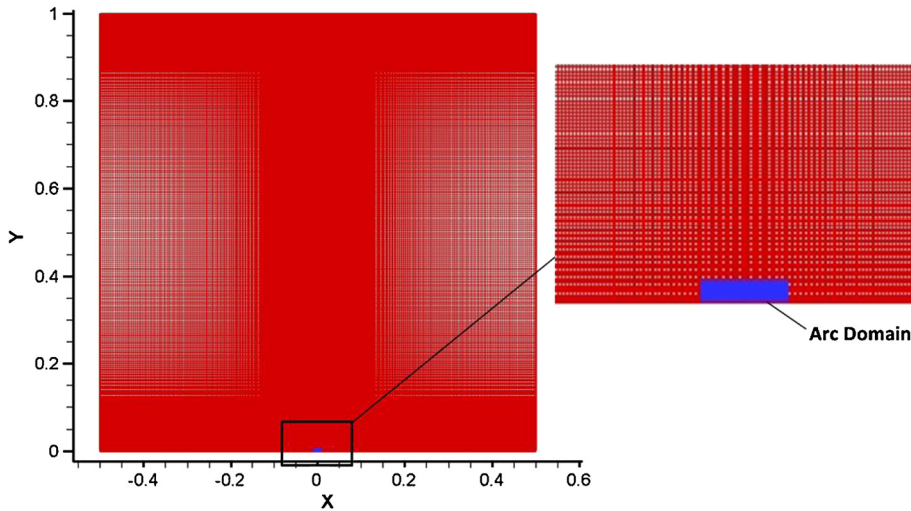


Fig. 10. Calculation mesh.

Here ρ , v , E and p are the density, velocity, total energy per unit mass, and pressure of the fluid, respectively. τ is the viscous stress tensor, and q is the heat flux. M_x , M_y and M_z are the momentum source caused by plasma accusation with current I , magnetic induction \mathbf{B} and cross section area \mathbf{S} . Since magnetic induction \mathbf{B} equals to zero for current research, all momentum source will remains to zero. E_s is heat source or power density of the plasma actuation in the unit of W/m^3 .

Millisecond actuation and microsecond actuation will be analyzed in present research. As shown in Fig. 9, t_1 is an arbitrary time during simulation and the entire actuation process is from 0 to t_2 . Since the investigation for the millisecond actuation is focus on the flow field during the first period, steady state assumption is used to simplify the numerical simulation. For the microsecond actuation, the period of the heat source is 1000 Hz. Transnet simulation is used and the source adds in the first 5 us of each period.

4.2. Turbulence model and Grid generation

To model the supersonic flow, various turbulence models are tested and the results indicate that the $k-\omega$ SST turbulent model is the most accurate model for the present problem. The detailed turbulent model is governed by the following two equations as:

$$\frac{\partial}{\partial t}(\rho k) + \frac{\partial}{\partial x_i}(\rho k u_i) = \frac{\partial}{\partial x_j} \left(\Gamma_k \frac{\partial k}{\partial x_j} \right) + G_k - Y_k + S_k \quad (3)$$

and

$$\frac{\partial}{\partial t}(\rho \omega) + \frac{\partial}{\partial x_i}(\rho \omega u_i) = \frac{\partial}{\partial x_j} \left(\Gamma_\omega \frac{\partial \omega}{\partial x_j} \right) + G_\omega - Y_\omega + S_\omega \quad (4)$$

In these equations, k is the turbulence kinetic energy, ω is the specific dissipation rate, G_k represents the generation of turbulence kinetic energy due to mean velocity gradients. G_ω represents the generation of ω . Γ_k and Γ_ω represent the effective diffusivity of k and ω respectively. Y_k and Y_ω represent the dissipation of k and ω due to turbulence. S_k and S_ω are source terms.

The calculating domain is a squared region with boundary length of 1 m as shown in Fig. 10. The heat source located in the middle of bottom boundary. Based on schlieren images, the cross section of arc domain is defined to be 5 mm (length) \times 2 mm (height).

4.3. Results

With the help of current numerical model, millisecond actuation and microsecond actuation were simulated under different power density. These numerical results will compared with experiment results. The influence of surface arc plasma on fluid field will also be investigated.

4.3.1. Simulation for millisecond actuation in supersonic flow

It is necessary to recall here, that the steady state assumption was used to simulate millisecond actuation. From the $V-I$ discharge characteristic of Fig. 2, two different power densities, $10^{10} \text{ W}/\text{m}^3$ and $10^{11} \text{ W}/\text{m}^3$, were tested. Fig. 11 illustrated the

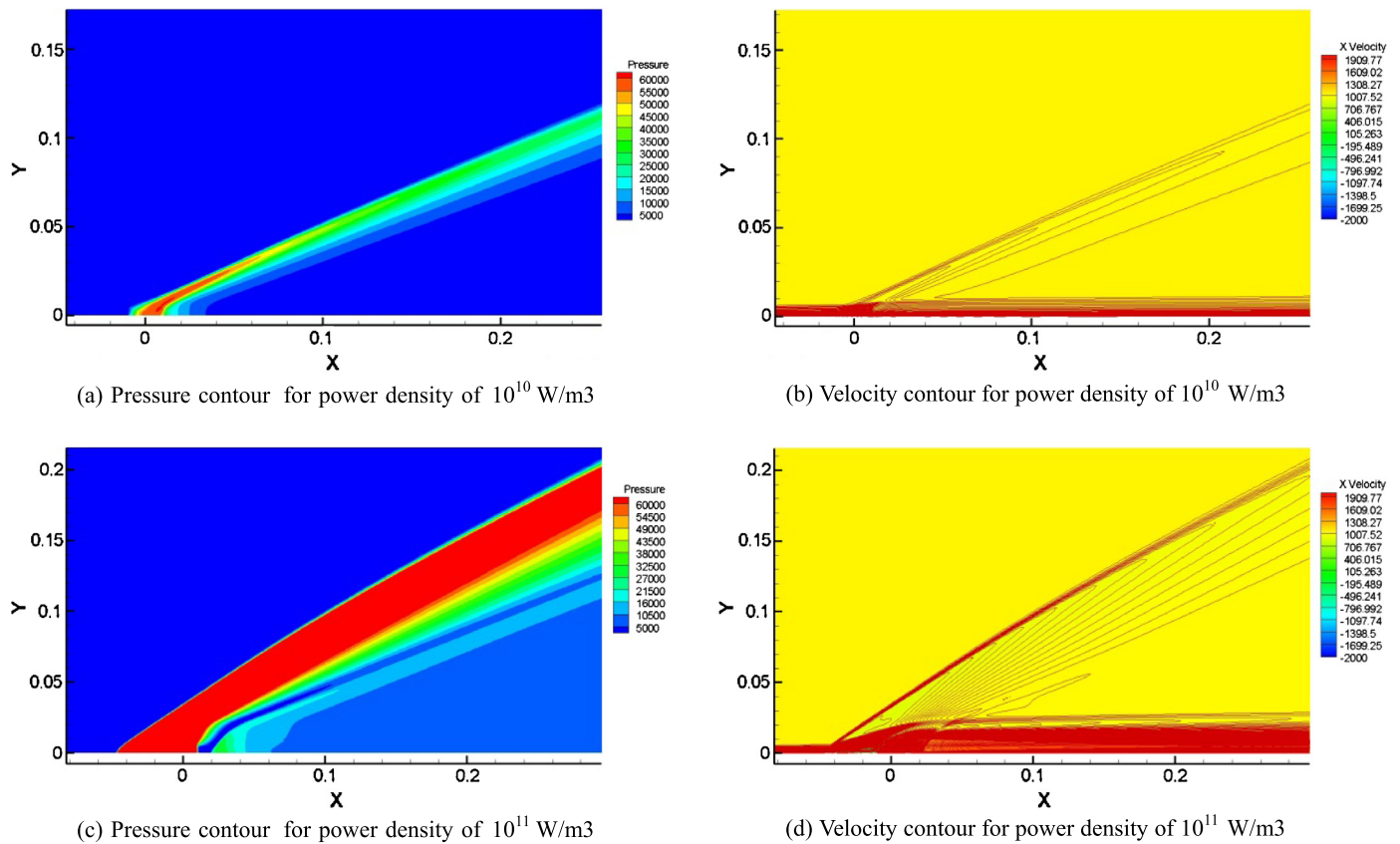


Fig. 11. Pressure and velocity contour for different power density.

pressure and velocity contour for different power density cases. An oblique shock wave induced by the millisecond actuation appears in the fluid field for both cases, which is coinciding with the experiment results.

The oblique shock wave for power density of 10^{10} W/m³, as shown in Fig. 11(a), is develop from the source region with the wave angle of 21.8 deg. With the increasing of the power density, the width of the oblique shock wave increases and its left boundary moves towards the upstream region which because of the heat block phenomenon. The strength of the shock wave under power density of 10^{11} W/m³ is higher than that under the power density of 10^{10} W/m³. By analyzing Fig. 11(c) and (d), a double oblique shock wave structure with a low pressure gap between them could be observed. The boundary layer is much wider after the shock wave.

Fig. 12 shows the pressure ratio and temperature distribution along X axis direction. From these figures, it is clear that the pressure and temperature step rise at the left boundary of the plasma source and drop down at the right boundary under power density of 10^{10} W/m³. By increasing the power density to 10^{11} W/m³, the pressure ratio and temperature starts to increase before the boundary of the heat source. The widths of the peak are also wider than that of the power density equals to 10^{10} W/m³ for both pressure ratio and temperature. The secondary oblique shock wave is also observed as a lower peak with a bottom value connected with the main shock wave.

4.3.2. Simulation for microsecond actuation in supersonic flow

In this section, the microsecond actuation in supersonic flow is tested. From the V-I discharge characteristic of Fig. 3, two different power densities, 10^{11} W/m³ and 10^{12} W/m³, were tested. The instantaneous pressure and temperature in the source region

[0.002, 0.002] and in the wake of the source region [0.012, 0.002] are also analyzed.

Fig. 13 shows the pressure contour in one period. At time instant of 5 μs, the high pressure region remains the rectangular shape as the heat source. The compressive wave develops as an arc shape and blows away to the downwind by the supersonic flow at time instant of 20 μs. At time point of 50 μs and 80 μs, the compressive wave continuously developing and moves to downwind. The strength of the compressive wave damped with the time flow.

From Fig. 14, the pressure and temperature development are different between source region and wake region. For both pressure and temperature development in source region, three stages could be observed which are increasing stage from 0 μs to 2 μs, peak stage from 2 μs to 5 μs and decrease stage. In the increasing stage, the pressure and temperature increasing suddenly and reach to its peak at 2 μs. In the peak stage, the pressure and temperature remains the peak value between 2 μs and 5 μs. In the decrease stage, the pressure and temperature drop and reach to constant value. In the contrast, the pressure and temperature development in the wake region only contains two stages without peak stage compared with that in source region. The peak value also delayed and lower than that in source region. In the decreasing stage, the pressure and temperature drops slowly and reach the constant value.

By increasing the power density, the strength of the compressive wave has enhanced. Fig. 16 shows that the structure of the compressive wave is more complex than that with the power density of 10^{11} W/m³. The shape of the arc is not an ideal half circle. The arc has small curvature in upwind part and large curvature in the downwind.

The pressure and temperature development in both source region and wake region are also different from that under power

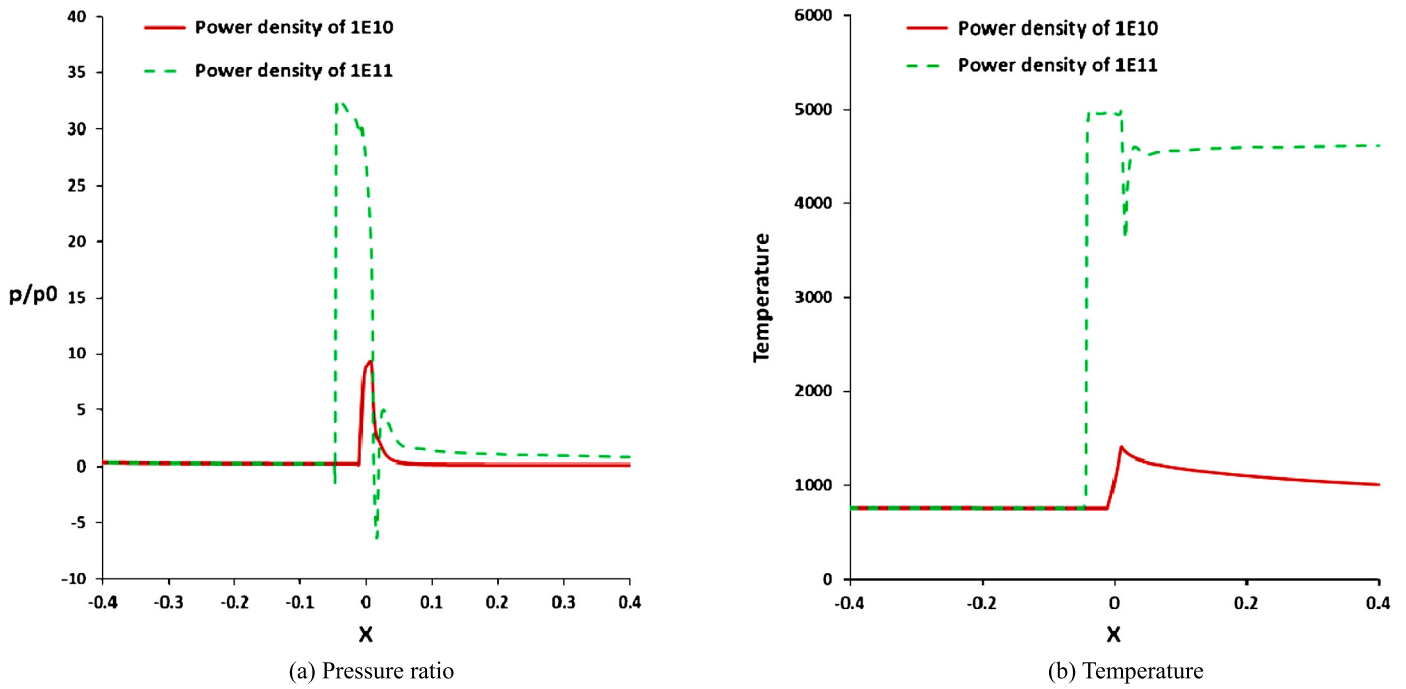


Fig. 12. Pressure ratio and temperature distribution along X axis direction.

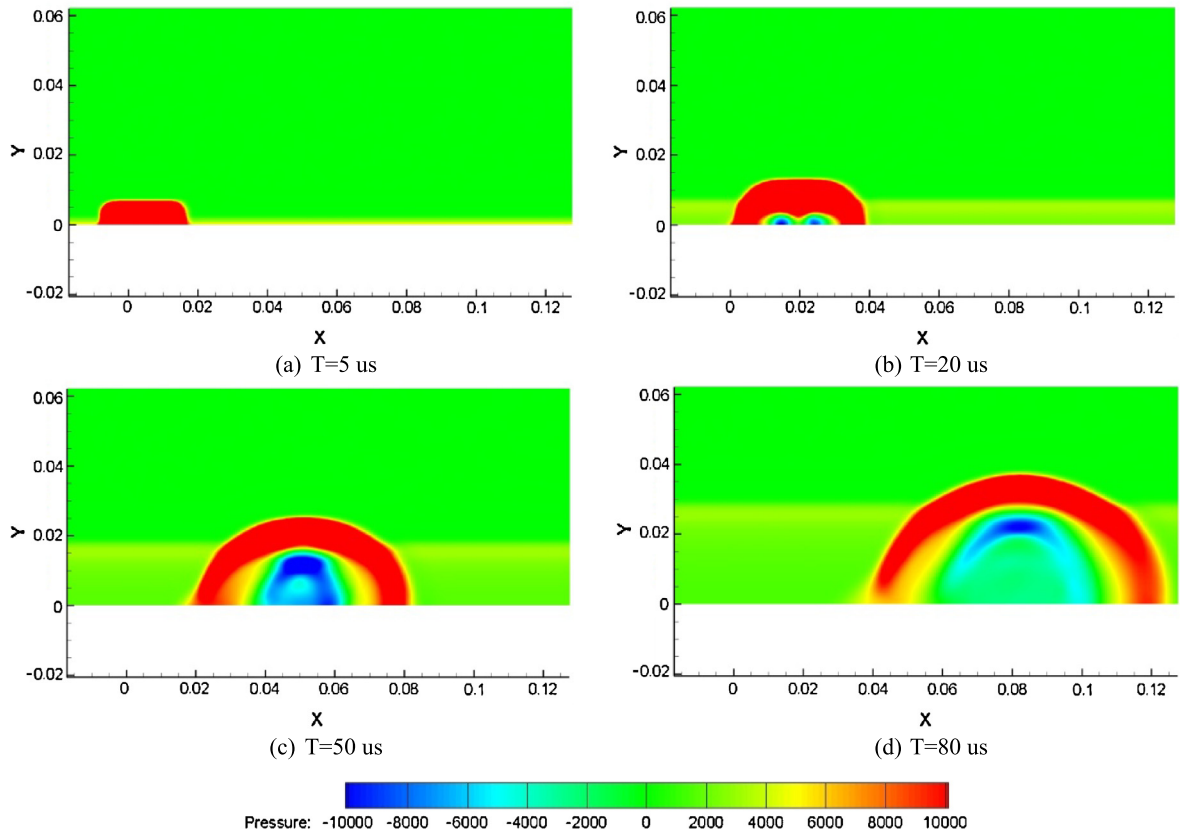


Fig. 13. Pressure contour within one period for power density of 10^{11} W/m^3 .

density of 10^{11} W/m^3 (Fig. 15). The peak value for pressure and temperature in both source and wake region are much higher, but the peak stage is shorter. The pressure and temperature difference on the peak value between source region and wake region is larger than that of low power density.

The radius of compressive wave arc is summarized in Table 1. It is clear that the size of the arc increase successively under certain power density. As the power density increase, the size of the arc is increase accordingly. That shows good agreement with our experiment results.

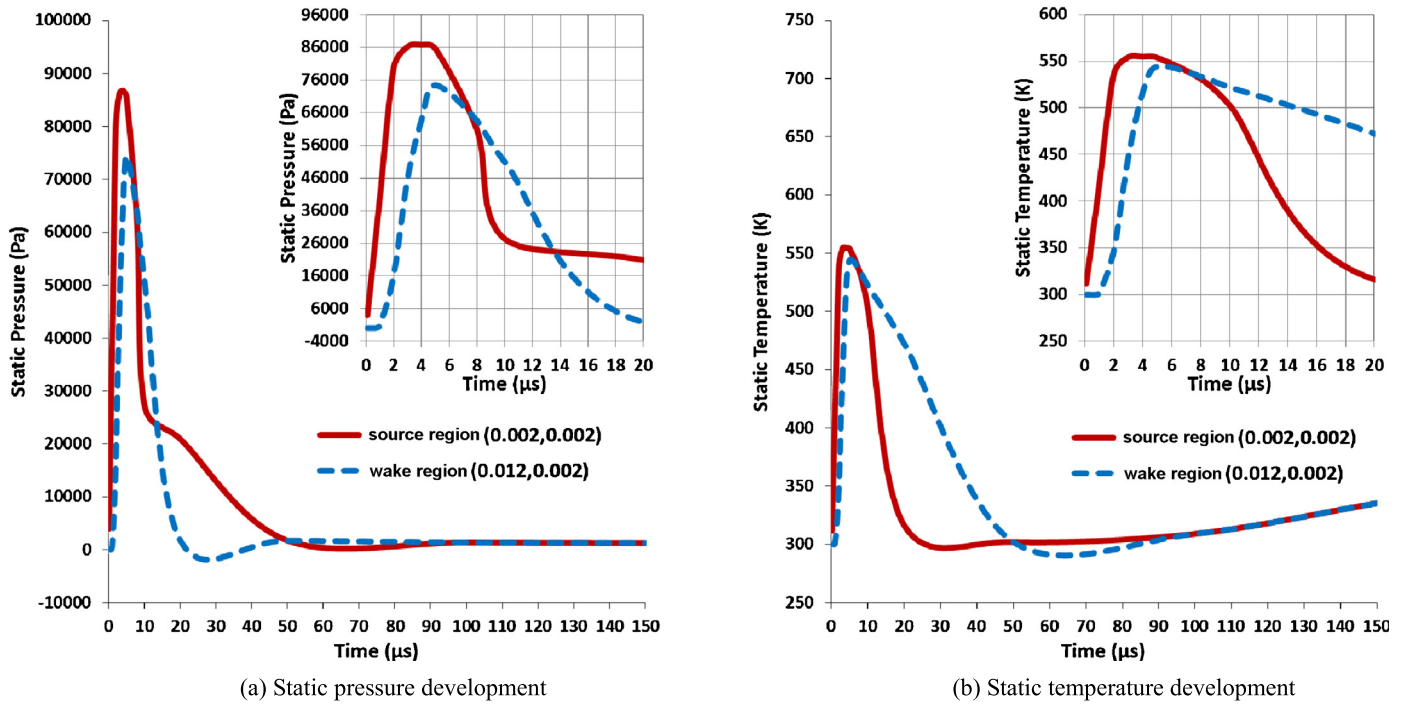


Fig. 14. Source region and wake region's static pressure and static temperature development for power density of 10^{11} W/m³.

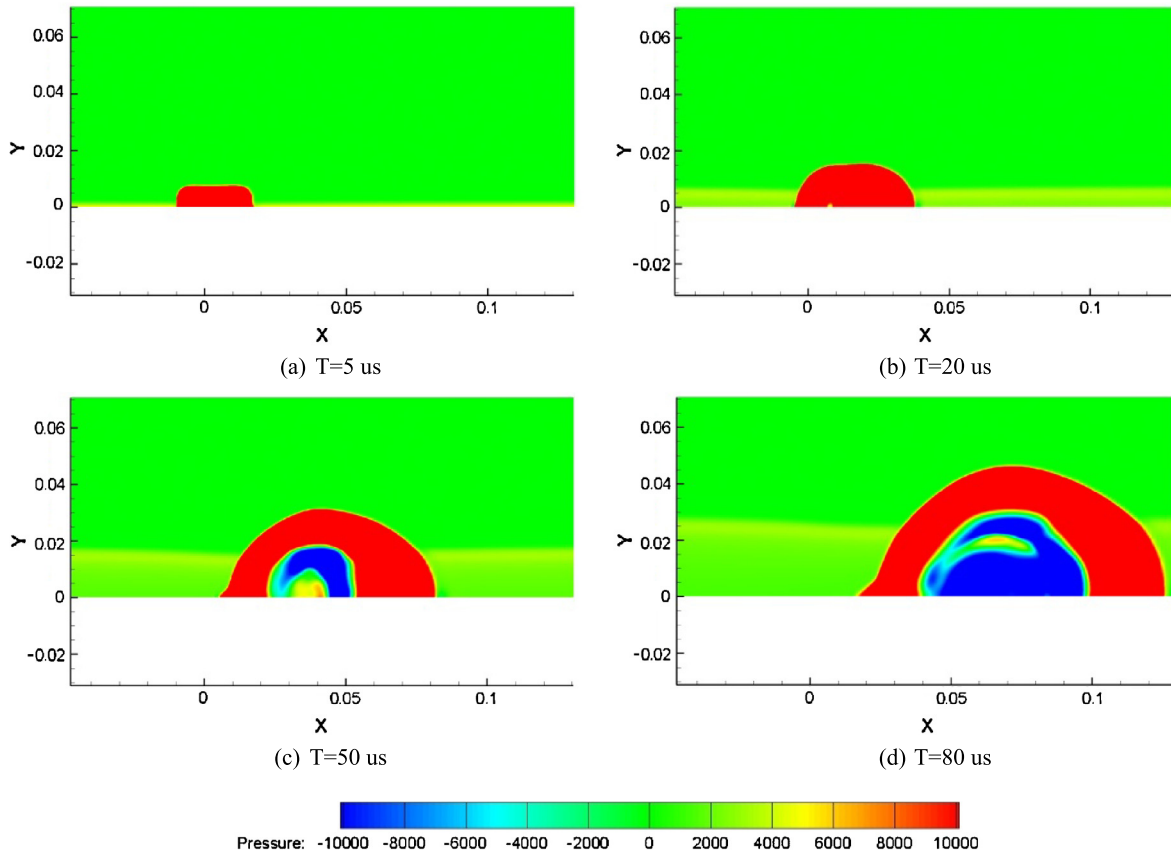
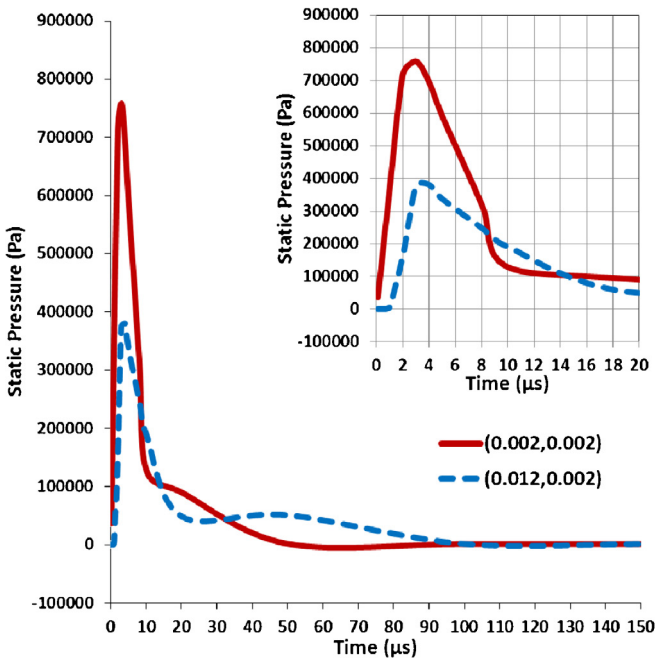


Fig. 15. Pressure contour within one period for power density of 10^{12} W/m³.

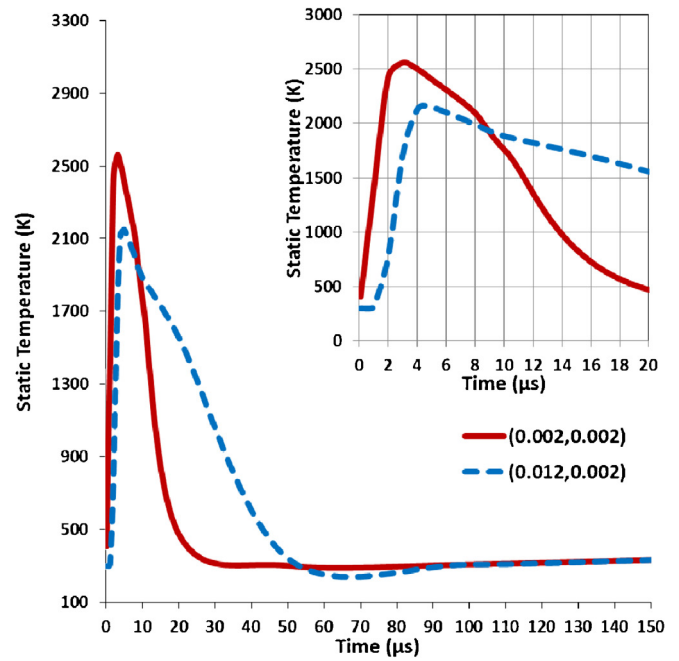
5. The application of surface arc discharge in supersonic flow

The dominating mechanism may be varied for different plasma sources or actuators. In this paper, two kinds of surface arc discharge are studied. The main control mechanism of millisecond

actuation is Joule heating. High temperature plasma generated changes the pressure and the temperature of near-wall region, forms virtual aerodynamic surface in a supersonic airstream. Millisecond actuation of arc plasma can induce shock in supersonic flow and make the air flow deflected after shock. The main control



(a) Static pressure development



(b) Static temperature development

Fig. 16. Static pressure and static temperature development for power density of 10^{12} W/m³.

Table 1

Radius of compressive wave arc in different instantaneous time and power density.

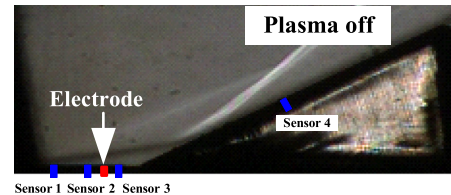
	$T = 5 \mu s$	$T = 20 \mu s$	$T = 50 \mu s$	$T = 80 \mu s$
$P = 10^{11}$ W/m ³	0.0075 m	0.0133 m	0.0254 m	0.0375 m
$P = 10^{12}$ W/m ³	0.0075 m	0.0155 m	0.0314 m	0.0463 m

mechanism of microsecond actuation is impact effect. Compression wave generated by the pulse discharge in the actuator is readily apparent in supersonic flow. The propagating compression wave produced by the discharge disturbs the oblique shock, and results in a perturbation when traveling along the shock.

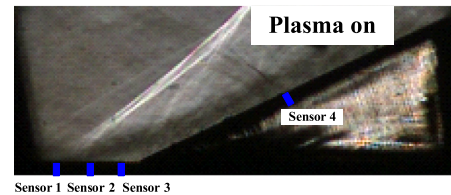
5.1. Experimental investigation on control shock intensity

In the case of oblique shock wave generated using a 25 deg ramp, there exists strong separation. From Fig. 17(a), the separation shock, the reattached shock, and the flow separation region near the bottom wall, can be identified clearly. The actuator is placed at the separation area. The plasma actuation in this setup results in some important change in the structure of the separation region. The electrodes located between sensor 2 and sensor 3. We used millisecond power supply to create the plasma actuation. The discharge characteristics are similarly with Fig. 2. From Fig. 17(b), the discharge causes the oblique shock to move upstream. The separation shock is no longer visible due to breakdown of shock foot. The separation phenomenon shifts backward and the size of separation enlarged when applying plasma aerodynamic actuation.

Four typical places were selected to measure static pressure of model. Static pressure measured uses wall pressure taps and the response frequency of pressure transducers is 100 kHz. Along the supersonic flow direction, there are 3 pressure dots (sensor 1, sensor 2, and sensor 3) which cover the interaction area of shock wave and boundary layer in Fig. 17. The flow is forced by the arc plasma actuation at the pulse repetition rate of 1 kHz. In Fig. 18(a), the pressure values of three sensors are approximately same. This result indicates that the flow is separated due to the interaction by oblique shock. When applying plasma actuation, the pressure value of sensor 1 is almost equal compared with baseline flow. But the



(a) The baseline flow



(b) The flow field with plasma actuation

Fig. 17. The flow field with and without plasma actuation.

pressure values of sensor 2 and sensor 3 increase along the supersonic flow in Fig. 18(b). In Fig. 18(c), the baseline wall static pressure profile is compared with plasma actuation. The baseline pressure is a plateau which indicates that the flow is separated due to the interaction. The slope increases rapidly as actuation is applied compared with the baseline which indicates that separation phenomenon shifts backward. The induced shock by arc discharge is apparent stronger than the separation shock of baseline flow. The effect of plasma actuation becomes more apparent and results in significant modification of the static wall pressure profile.

The intensity of shock wave is denoted by the ratio between the static pressure after shock wave and undisturbed static pressure. Fig. 19 is the curve of shock wave intensity which is the ratio between sensor 4 and sensor 1. From the picture, the intensity of shock wave is apparent reduced by plasma aerodynamic actuation. The main reason is that the structure of shock wave is changed. The arc discharge changes the strong reattached shock into two

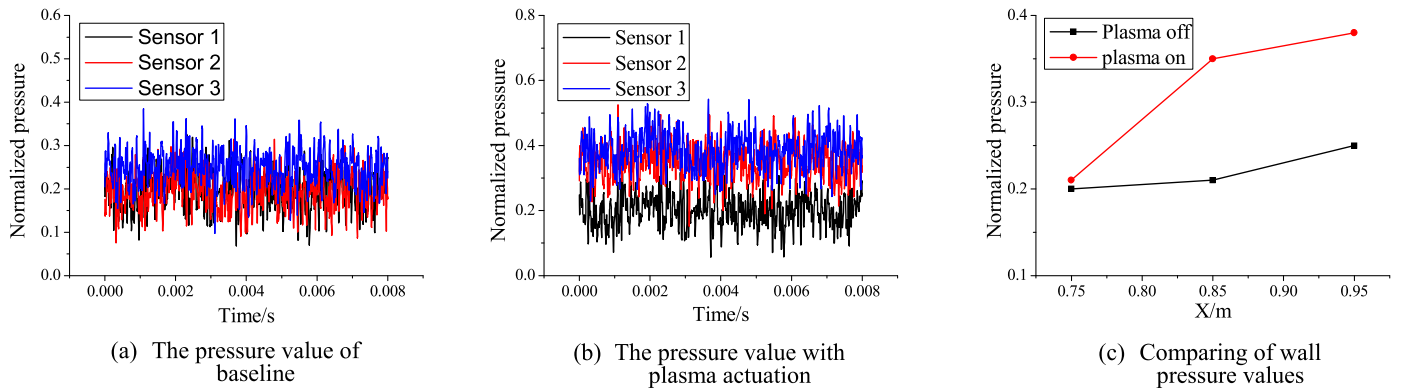


Fig. 18. The pressure value of wall separation area.

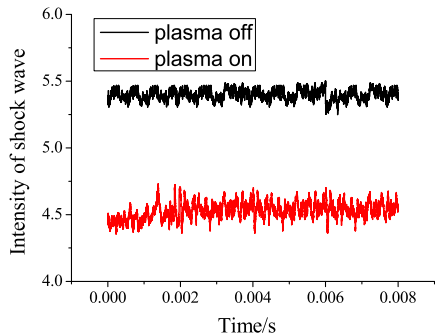


Fig. 19. The intensity of shock wave with plasma aerodynamic actuation.

oblique shocks. So, the intensity of shock wave is weakened by 18% compared with baseline flow.

5.2. Experimental investigation on control boundary layer separation

Fig. 20(a) shows one phase-locked schlieren image of the baseline flow. The flow Mach is 3 and the ramp is 15 deg. This is consistent with the oblique shock angle of 32 degree. In the image, the incident shock, the reflected shock, and the flow separation region near the bottom wall, can be identified clearly. The impinging shock front disappears at the intersection with the sonic line, encompassing the separated flow region. The incoming boundary layer on the lower wall appears to be turbulent, with a boundary layer thickness of approximately 3 mm. We used microsecond power supply to create the plasma actuation. The discharge characteristics are similarly with Fig. 3. The actuator is placed at just upstream of the front leg of the lambda shock. Fig. 20(b) shows one phase-locked schlieren image taken when the flow is forced by the plasma actuator at the pulse repetition rate of 2 kHz. In the case of oblique shock wave generated using a 15 degree ramp, there exists strong separation and upstream plasma actuation in this setup results in increased recirculation as expected. This result shows that the arc plasma actuation can restrain or delay the separation.

Static pressure measured uses wall pressure taps. Along the supersonic flow direction, there are 3 pressure dots (sensor 1, sensor 2, and sensor 3) which cover the interaction area of shock wave and boundary layer. In Fig. 21(a), the pressure values of three sensors are approximately same. This result indicates that the flow is separated due to the interaction by impinging shock. When applying plasma aerodynamic actuation, the pressure value increases along the supersonic flow in Fig. 21(b). The effect of plasma actuation becomes more apparent and results in significant modification of the static wall pressure profile.

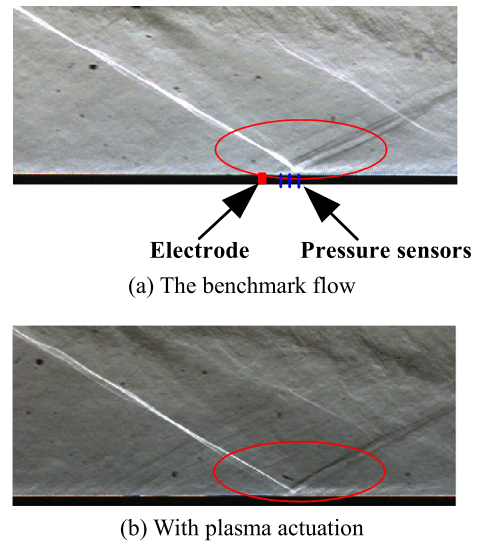


Fig. 20. The schlieren images without and with plasma actuation.

As we all know, low frequency, large amplitude unsteadiness of a broadband nature has been observed in the region around the foot of the reflected shock. When actuation frequency of plasma-shock is consistent with the nature oscillations frequency of SWB-LIs, plasma-shock maybe controls the separation of boundary layer. The compressive wave induced by plasma actuation is observed in Fig. 22. The propagating compression wave produced by the discharge disturbs the oblique shock wave, and results in a perturbation when traveling along the shock. The actuators are operated at several different forcing frequencies (800 Hz, 1000 Hz, 1200 Hz, 1500 Hz and 2000 Hz) to determine the best control authority. There appears to be no resonance or optimal frequency associated with this actuator. Due to the limit of plasma power frequency (only 100 Hz–2000 Hz), further studies are required to be finished for higher frequency to validate this idea.

6. Conclusion and future work

The characteristic of surface arc plasma included millisecond and microsecond actuation in supersonic flow is investigated both experimentally and numerically. All results show that it can induce oblique shock with millisecond surface arc plasma actuation and can induce compressive wave with microsecond surface arc plasma actuation. In the shock induced by ramp control, the shock intensity is reduced, but separation of boundary layer is enlarged by millisecond surface arc plasma actuation. In the separation of boundary layer control, the size of separation area induced by impinging shock is reduced. All the results demonstrate the control

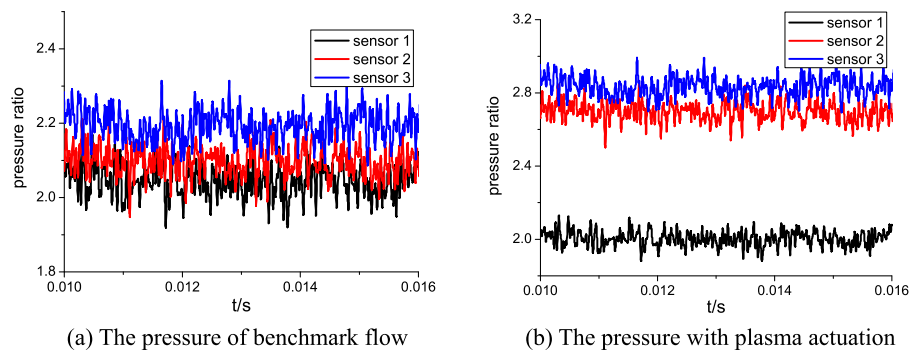


Fig. 21. The pressure value of wall separation area.

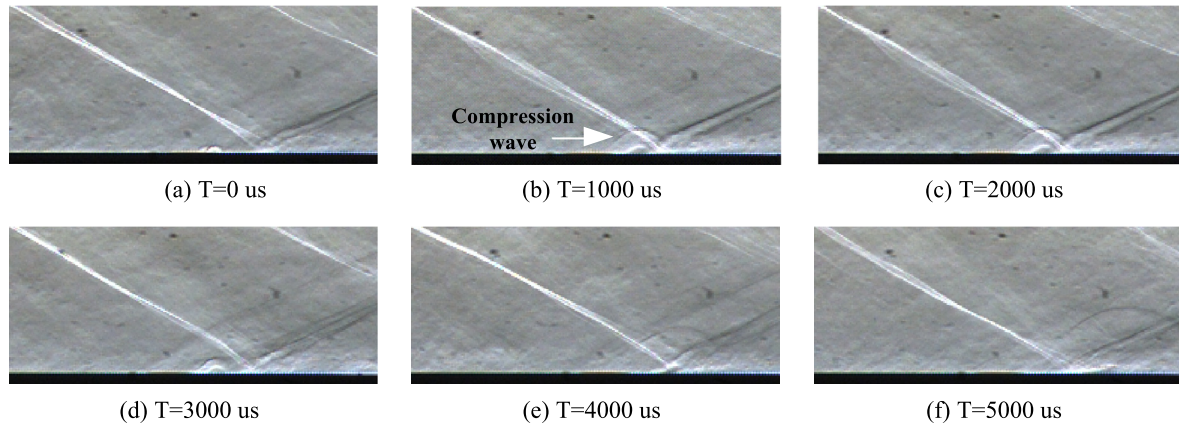


Fig. 22. Compression wave induced in supersonic flow.

authority of surface arc plasma actuation onto supersonic flow. The primary control mechanism is through heating induced oblique shock and compressive wave by surface arc plasma actuation.

Future work should focus on the control mechanism of shock and compressive wave induced by surface arc plasma disturbing the supersonic flow. Besides, some adjustment is necessary to improve the numerical model in order to optimize the parameter and structure of actuator.

Acknowledgements

The research was supported by the Key Program of the National Natural Science Foundation of China (Grant No. 51336011) and the National Natural Science Foundation of China (Grant Nos. 51207169 and 11372352) and is gratefully acknowledged.

References

- [1] J.R. Roth, *Phys. Plasmas* 10 (2003) 2117.
- [2] J.R. Roth, D.M. Sherman, *AIAA J.* 38 (2000) 116.
- [3] T.C. Corke, M.L. Post, D.M. Orlov, *Exp. Fluids* 46 (2009) 1.
- [4] S.B. Leonov, D.A. Yarantsev, *J. Propuls. Power* 24 (2008) 1168.
- [5] J. Wang, Y.H. Li, B.Q. Cheng, C.B. Su, H.M. Song, Y. Wu, *J. Phys. D, Appl. Phys.* 42 (2009) 165503.
- [6] S.B. Leonov, *ASTIA Documents A*, 2005, 433384.
- [7] S.B. Leonov, V. Bityurin, K. Savelkin, D. Yarantsev, in: *33rd Plasma Dynamics and Lasers Conference*, 2002, p. 2180.
- [8] D. Knight, O. Azarova, Y. Kolesnichenko, in: *47th AIAA Aerospace Sciences Meeting Including the New Horizons Forum and Aerospace Exposition*, 2009, p. 847.
- [9] D. Knight, V. Kuchinsky, A. Kuranov, E. Sheikin, in: *41st Aerospace Sciences Meeting and Exhibit*, 2003, p. 525.
- [10] R. Meyer, P. Palm, E. Ploenjes, in: *Proceedings of the 32nd AIAA Plasma Dynamics and Lasers Conference*, 2001, p. 3059.
- [11] N. Webb, C. Clifford, M. Samimy, in: *51st AIAA Aerospace Sciences Meeting Including the New Horizons Forum and Aerospace Exposition*, 2013, p. 0402.
- [12] N. Webb, C. Clifford, M. Samimy, in: *6th AIAA Flow Control Conference*, 2012, p. 2810.
- [13] N. Webb, C. Clifford, M. Samimy, in: *41st AIAA Fluid Dynamics Conference and Exhibit*, 2011, p. 3426.
- [14] E. Caraballo, N. Webb, J. Little, M. Samimy, in: *47th AIAA Aerospace Sciences Meeting Including the New Horizons Forum and Aerospace Exposition*, 2009, p. 924.
- [15] C.S. Kalra, S.H. Zaidi, R.B. Miles, S.O. Macheret, *Exp. Fluids* 50 (2011) 547.
- [16] C.S. Kalra, S.H. Zaidi, M.N. Shneider, R.B. Miles, in: *47th AIAA Aerospace Sciences Meeting Including the New Horizons Forum and Aerospace Exposition*, 2009, p. 1002.
- [17] V. Narayanaswamy, L.L. Raja, N.T. Clemens, *Phys. Fluids* 24 (2012) 076101.
- [18] M. Nishihara, D. Gaitonde, I.V. Adamovich, in: *51st AIAA Aerospace Sciences Meeting Including the New Horizons Forum and Aerospace Exposition*, 2013, p. 0461.
- [19] Q. Sun, B.Q. Cheng, Y.H. Li, *Plasma Sci. Technol.* 15 (9) (2013) 908–914.
- [20] Q. Sun, B.Q. Cheng, Y.H. Li, *Sci. China, Technol. Sci.* 56 (4) (2013) 795–802.
- [21] Q. Sun, B.Q. Cheng, Y.H. Li, *Plasma Sci. Technol.* 15 (11) (2013) 1136–1143.
- [22] J. Wang, B.Q. Cheng, Y.H. Li, *J. Appl. Phys.* 106 (2009) 073307.